Microwave-Driven Atoms: From Anderson Localization to Einstein's Photoeffect

Alexej Schelle,[1,2] Dominique Delande,[2] and Andreas Buchleitner[1]

[1]*Physikalisches Institut der Albert-Ludwigs-Universität, Hermann-Herder-Strasse 3, D-79104 Freiburg, Germany*

[2]*Laboratoire Kastler-Brossel, Université Pierre et Marie Curie-Paris 6, ENS, CNRS; 4, Place Jussieu, F-75005 Paris, France*

(Received 5 September 2008; published 4 May 2009)

We study the counterpart of Anderson localization in driven one-electron Rydberg atoms. By changing the initial Rydberg state at fixed microwave frequency and interaction time, we numerically monitor the crossover from Anderson localization to the photoeffect in the atomic ionization signal.

DOI: 10.1103/PhysRevLett.102.183001 PACS numbers: 32.80.Rm, 05.60.Gg, 32.80.Wr, 71.23.−k

Anderson localization [1,2] is the inhibition of quantum transport due to destructive interference in disordered, static quantum systems. When a Hamiltonian quantum system is periodically driven and its classical counterpart undergoes a transition to chaotic diffusion, an analogous localization phenomenon occurs: destructive interference between many chaotically diffusing trajectories inhibits the transport and localizes the diffusing particle's wave function [3]. Since dynamical chaos rather than static disorder establish Anderson's scenario here, the phenomenon is often labeled *dynamical* localization.

Until now, the dynamical variant of Anderson localization (and similar phenomena [4]) was observed in a vast range of physical systems—ranging from cold atoms [5] to photon billiards [6] and atoms [7–10], and is best understood in the Floquet or dressed state picture, which also allows its formal mapping on Anderson's model [11]. The dressing of the bare system by the driving field photons defines multiphoton transition amplitudes between the initial and the final field-free state, mediated by near-resonantly coupled intermediate states. These amplitudes need be summed up coherently to determine the total transport probability. For *destructive* interference and thus localization to emerge, a *large* number of amplitudes is required, what implies that the photon energy be *small* compared to the energy gap between initial and final state. This is a scenario in perfect contrast to Einstein's photoeffect [12], which predicts *efficient* transport—mediated by *one single* transition amplitude—for photon energies *larger* than that energy gap, though the general physical context of a driven quantum system is identical in both cases. Recently, connecting both effects through continuous variation of the experimental parameters has moved into reach for state-of-the-art atomic physics experiments [13], and it is the purpose of this Letter to (theoretically) establish this connection and to spell out its characteristic features.

Our specific atomic physics scenario is defined by a one-electron Rydberg atom under periodic driving by a classical, linearly polarized oscillating electric field of amplitude F and frequency ω, described (in length gauge and atomic units, employing the dipole approximation) by the Hamiltonian

$$H(t) = \frac{\mathbf{p}^2}{2} - \frac{1}{r} + \mathbf{F}\cdot\mathbf{r}\cos(\omega t), \tag{1}$$

with $\mathbf{p}$ and $\mathbf{r}$ the electron's momentum and position, respectively. In this system, quantum transport properties are efficiently characterized by the ionization probability $P_{\mathrm{ion}}(t)$ after a given atom-field interaction time t, for an atomic initial state $|\Phi_0\rangle = |n_0, \ell_0, m_0\rangle$ with well-defined principal and angular momentum quantum numbers n_0, ℓ_0, and m_0 (the latter one being a constant of motion for linearly polarized driving). Transport occurs on the energy axis, from the bound initial state towards asymptotically free continuum states, and is mediated by the absorption of at least

$$N_{\rightsquigarrow} = \frac{1}{\omega}\left(\frac{1}{2n_0^2} - \frac{1}{2n_{\mathrm{eff}}^2}\right) = \frac{1}{2\omega n_0^2}\left(1 - \frac{n_0^2}{n_{\mathrm{eff}}^2}\right) \tag{2}$$

photons by the electron from the driving field, where $n_{\mathrm{eff}} < \infty$ denotes the *effective ionization threshold* (at negative energy $-1/2n_{\mathrm{eff}}^2$). The latter is fixed by the specific experimental conditions and caused by unavoidable experimental imperfections such as electric stray fields. A typical value for state-of-the-art experiments is $n_{\mathrm{eff}} \simeq 270$ [10,13,14], which we will employ throughout the remainder of this Letter. Since, at a given laboratory driving field frequency $\omega = 2\pi \times 17.5$ GHz [13], all field-free bound states with $n_{\mathrm{eff}} > n_0 \geq 230$ will be coupled directly to the atomic continuum by *one single photon*, such an experimental ionization threshold allows for the continuous interpolation between the Anderson limit and the photoeffect as described above. It suffices to monitor $P_{\mathrm{ion}}(t)$ as a function of n_0, with all other experimental parameters fixed.

We will now model such a scan by a faithful numerical description of the atomic system under study. Our theoretical or numerical tool box is described in detail elsewhere [15,16]. We only recall here that the theoretical approach combines Floquet theory [17] and complex dilation of the Hamiltonian [18,19], possibly amended by R-matrix theory to account for the multielectron core of alkali Rydberg states [15], together with considerable

computational power provided by parallel supercomputing facilities. The production of one single data point as displayed in the figures below requires repeated diagonalization of banded complex symmetric matrices of dimension up to 10^6, which amounts to storage needs up to 150 GB.

In order to highlight the continuous transition from suppressed transport due to Anderson localization to enhanced transport due to the photoeffect, we scan an energy range of atomic initial states from $n_0 = 90$ to $n_0 = 245$, at fixed microwave frequency and atom-field interaction time $t = 500$ ns, and angular momentum quantum numbers $\ell_0 = 1$, $m_0 = 0$. The specific choice of these parameters is inspired by ongoing experiments [13] on Rydberg states of lithium, and we will provide data for lithium as well as for atomic hydrogen, to disentangle universal features of the said transition from those characteristic of the atomic species under scrutiny. Furthermore, our ''starting value'' $n_0 = 90$ guarantees that we start out in the Anderson regime, where the ionization yield is characterized by a universal ionization threshold *irrespective* of the atomic species [20].

Figure 1 shows the results of our calculation in terms of the scaled ionization threshold field $F_0^{10\%} = F^{10\%} n_0^4$, i.e., of the driving field amplitude $F_0^{10\%}$ which induces

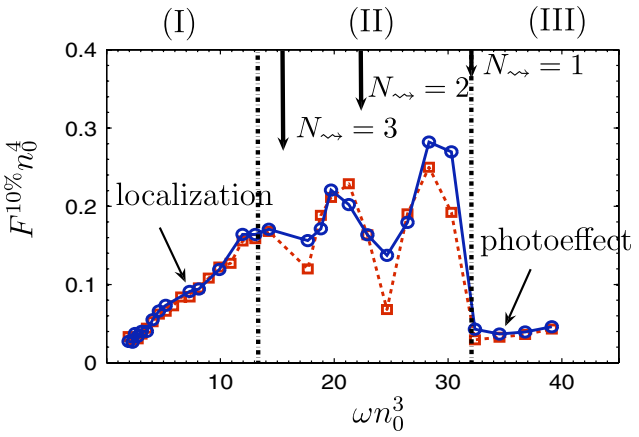

FIG. 1 (color online). Scaled ionization threshold field $F_0^{10\%} = F^{10\%} n_0^4$ of atomic hydrogen [red dashed line (□)] and lithium [blue solid line (○)], at fixed laboratory microwave frequency $\omega = 17.5$ GHz and interaction time $t = 500$ ns. The scaled frequency $\omega_0 = \omega n_0^3 = 1.9$–$39.1$ is tuned by changing the initial state's principal quantum number from $n_0 = 90$ to $n_0 = 245$, at fixed values of the angular momentum quantum numbers $\ell_0 = 1$ and $m_0 = 0$. We observe three distinct regimes. (I), $1.9 \leq \omega_0 \leq 13.1$: the monotonous increase of $F_0^{10\%}$ with ω_0 is a characteristic signature of Anderson localization in strongly driven quantum systems [20]. Regime (II), $13.1 \leq \omega_0 < 31.5$: $F_0^{10\%}$ still increases with ω_0, on average, but is garnished by large modulations due to the passage of the atomic initial state across subsequent $N_{\rightsquigarrow}$-photon ionization thresholds indicated by vertical arrows. Anderson localization and finite $N_{\rightsquigarrow}$-photon ionization coexist. Regime (III), $\omega_0 \geq 31.5$: The photon energy exceeds the ionization potential of the initial state, the Anderson scenario is inapplicable, and single photon absorption mediates the ionization process.

$P_{\rm ion}(t) = 0.1$, measured in units of the Coulomb field experienced by the electron on its unperturbed Rydberg orbit n_0 [21]. The threshold field is plotted as a function of the scaled driving field frequency $\omega_0 = \omega n_0^3$, i.e., of the driving field frequency ω measured in units of the unperturbed Kepler frequency for n_0. Clearly, we can identify three regimes of qualitatively different behavior: In regime (I), for low principal quantum numbers $n_0 = 90$–170 (corresponding to scaled frequencies $\omega_0 \simeq 1.9$–13.1), we witness the characteristic signature of Anderson localization—the scaled ionization threshold *increases* with the excitation of the initial atomic state, i.e., with *decreasing* ionization potential, and is essentially independent of the atomic species [20]. In regime (II), the ionization threshold still increases on average—suggestive of Anderson localization—but is garnished by large-scale modulations. Closer inspection of this oscillating structure reveals its origin in successive passages through the multiphoton ionization thresholds indicated by vertical arrows in the figure: The opening of a direct, $N_{\rightsquigarrow}$-photon ionization channel [22] is manifest in a local, rapid decrease of $F_0^{10\%}$ with ω_0 (since the dominant contribution to the ionization signal is of lower order). As ω_0 increases further on, the threshold field increases again, since the cross section for $N_{\rightsquigarrow}$-photon ionization decreases with increasing frequency—until the next channel opens. The thus emerging structures are precursors of the final opening of the single photon ionization channel at $n_0 = 230$ ($\omega_0 = 32.4$), which defines the demarcation line between regime (II) and the realm of the photoeffect, regime (III) [23].

We therefore witness a synchronicity of Anderson localization and ($N_{\rightsquigarrow}$-order) photoeffect in regime (II): the former still largely suppresses the ionization process, even when, by virtue of the value of $N_{\rightsquigarrow}$, multiphoton transitions of very low order mediate the transport, while the latter is already reflected in prominent nonmonotonicities of the threshold field. Only in regime (III) is Anderson localization completely absent.

A complementary analysis corroborates this interpretation. According to the theory of Anderson localization, the exponential localization of the electronic wave function on a characteristic scale ξ (in units of the driving field photon energy $\hbar\omega$) on the energy axis [24] implies an exponential scaling of the ionization yield, according to $P_{\rm ion} \sim \exp(-2N_{\rightsquigarrow}/\xi)$. Consequently, for a fixed ionization yield (as implicit in the definition of $F_0^{10\%}$), this leads to the prediction that $\xi(\omega_0, F_0^{10\%})/N_{\rightsquigarrow}$ be *independent* of ω_0. This is what is observed in Fig. 2 in regime (I) (modulo threshold fluctuations which are characteristic for the Anderson problem [25]), where we plot $\xi(\omega_0, F_0^{10\%})/N_{\rightsquigarrow}$ vs ω_0, with ξ estimated according to [24]

$$\xi \simeq 3.33 F_0^2 \omega_0^{-10/3} n_0^2. \tag{3}$$

This simple expression is known to be quantitatively incorrect [10,16], but to provide a qualitatively reliable

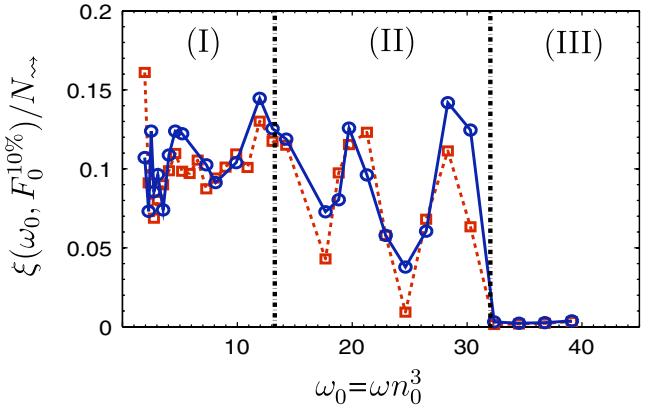

FIG. 2 (color online). Ratio of the atomic localization length ξ as estimated by Eq. (2) to the number of absorbed photons $N_{\rightsquigarrow}$, versus scaled frequency $\omega_0 = \omega n_0^3$. Data are extracted from the 10%-ionization thresholds of Fig. 1, for atomic hydrogen [red dashed line (□)] and lithium [blue solid line (○)]. On average, $\xi/N_{\rightsquigarrow}$ is constant in regime (I)—a hallmark of exponential localization of the electronic wave function on the energy axis. This is still true in regime (II), where, however, the discreteness of the lattice (on the energy axis) strongly affects the transport behavior: Large-scale modulations of the signal emerge due to direct $N_{\rightsquigarrow}$ photon transitions to the continuum. Only in regime (III) does ξ drop to zero, thus invalidating the Anderson picture.

characterization of the general trend of ξ with n_0. Furthermore, Fig. 2 clearly spells out that exponential localization of the electronic wave function on the energy axis prevails, at least on average, even deeply into regime (II), where the ionization behavior is simultaneously strongly affected by the described opening of few-photon ionization channels. In the Anderson picture, the latter is tantamount to finite size effects which manifest in localization lengths ξ of order unity, thus resolving the granularity of the lattice (on the energy axis) along which transport occurs. In regime (III), the lattice constant (i.e., here, the photon energy [11,24]) is larger than the effective sample length, and the Anderson picture turns inapplicable.

Let us finally analyze the characteristics of the atomic transport process in terms of its "complexity," which can be characterized in terms of the number of Floquet eigenstates which mediate the ionization process—which in turn provides a measure of the volume of Hilbert space which is effectively explored in the course of the ionization process. A good estimate thereof is given by the Shannon width [26]

$$\mathcal{W}(F_0^{10\%}, \omega_0) = \exp\Big[-\sum_j |w_j|^2 \ln|w_j|^2\Big], \qquad (4)$$

which raises the Shannon entropy of the decomposition $|\Phi_0\rangle = \sum_j w_j |\epsilon_j\rangle$ of the atomic initial state in the Floquet basis $\{|\epsilon_j\rangle\}$, with individual weights $|w_j|^2$ [25], to the number of Floquet states which effectively contribute. According to our qualitative understanding of Anderson localization on the one hand and the photoeffect on the other, the former is the consequence of the destructive interference of a *large* number of multiphoton transition amplitudes, while the latter is mediated by essentially *one single* transition matrix element. Consequently, Anderson localization implies the coupling of a large number of states, and this is tantamount to the spreading of the field-free atomic initial state over a large number of atomic eigenstates *in* the field, whereas in the photoeffect the atomic initial state is directly coupled to the continuum, without the participation of other bound states. Correspondingly, the Shannon width should be large in one case and small, rather close to 1, in the other. Figure 3 confirms this expectation: As a function of ω_0, at fixed laboratory value ω, the Shannon width exhibits large values in regime (I), and decreases almost monotonically to a level close to unity in regime (III), with intermediate values around approximately 20 in regime (II). Much as in our previous analysis of the ionization threshold's and the localization length's dependence on the scaled frequency, it is also here evident that the interference of multiple transition amplitudes as the fundamental mechanism of Anderson localization prevails very far into regime (II), even in the presence of already relatively efficient direct continuum coupling through few-photon ionization channels. The relatively high level of $\mathcal{W} \simeq 20$ even at $\omega_0 \simeq 30$ convincingly demonstrates the rapid proliferation of multiphoton coupling amplitudes as the photon energy becomes smaller than the initial state's ionization potential. In terms of the Anderson model, even small lattices suffice for the emergence of Anderson-like suppression of diffusive transport.

Figure 3 also highlights some subtle differences of the ionization process for different atomic species–here, lithium and atomic hydrogen: In regime (I), $\mathcal{W}$ is significantly

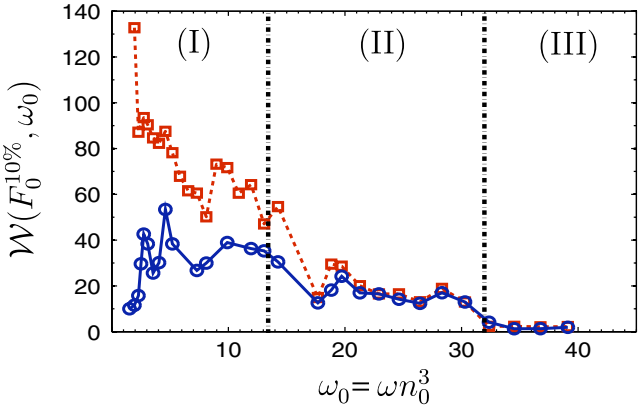

FIG. 3 (color online). Shannon width, Eq. (4), at the 10%-ionization threshold, as a function of the scaled frequency $\omega_0 = \omega n_0^3$, for the same parameters as in Fig. 1. Remarkably, $\mathcal{W}$ takes appreciable values for initial states up to right below the single photon ionization threshold at the lower edge of regime (III). In regime (I), atomic hydrogen exhibits considerably larger values than lithium, which we attribute to the angular momentum degeneracy of the hydrogenic initial state.

larger for hydrogen than for lithium, which we attribute to the higher degeneracy of the hydrogen atom's initial state's angular momentum manifold as compared to the nonhydrogenic initial state of lithium ($m_0 = 0$ renders $\ell = 0$ directly accessible by single photon absorption from $\ell_0 = 1$) [27]. The progressive vanishing of this discrepancy in regime (II) is consistent with the reduction of $N_{\rightsquigarrow}$.

In summary, we established a continuous transition from Anderson localized quantum transport to the photoeffect, by simple tuning of the sample length at fixed lattice constant, which, in our specific, experimentally relevant example from atomic physics, is defined by the ionization potential of the atomic initial state $|n_0, l_0, m_0\rangle$ and the energy $\hbar\omega$ of the injected photons, respectively. We have seen that both transport mechanisms coexist in a certain parameter range, where Anderson localization is garnished by finite size effects, which, in an atomic physics language, is nothing but the opening of multiphoton ionization channels. Our most remarkable observation is probably that characteristic signatures of Anderson localization prevail in the ionization signal even when absorption of very few photons suffices to ionize the Rydberg electron: Thus, quasirandomness as a necessary prerequisite of Anderson localization is rapidly established, if only the local spectral density permits the coupling of many unperturbed atomic states by comparably few photons.

We thank Joshua Gurian, Haruka Maeda, and Tom Gallagher for helpful discussions, and LRZ at the Bavarian Academy of Sciences, RZG of the Max Planck Society, and IDRIS Paris for providing computation time. A. S. and A. B. are grateful for partial funding through DFG (Forschergruppe 760), and A. S. acknowledges financial support through the QUFAR Marie Curie Action MEST-CT-2004-503847.

Note added.—Recently, we learned that the predicted ionization behavior in regime (II) was recently observed experimentally [13].

[1] P. W. Anderson, Phys. Rev. **109**, 1492 (1958).
[2] M. Störzer, P. Gross, C. M. Aegerter, and G. Maret, Phys. Rev. Lett. **96**, 063904 (2006); T. Schwartz, G. Bartal, S. Fishman, and M. Segev, Nature (London) **446**, 52 (2007); G. Roati, C. D'Errico, L. Fallani, M. Fattori, C. Fort, M. Zaccanti, G. Modugno, M. Modugno, and M. Inguscio, Nature (London) **453**, 895 (2008); J. Billy, V. Josse, Z. Zuo, A. Bernard, B. Hambrecht, P. Lugan, D. Clément, L. Sanchez-Palencia, Ph. Bouyer, and A. Aspect, Nature (London) **453**, 891 (2008); J. Chabé *et al.*, Phys. Rev. Lett. **101**, 255702 (2008).
[3] G. Casati, B. V. Chirikov, J. Ford, and F. M. Izrailev, *Stochastic Behavior in Classical and Quantum Hamiltonian Systems*, Lecture Notes in Physics Vol. 93 (Springer, New York, 1979), p. 334.
[4] E. Person, S. Fürthauer, S. Wimberger, and J. Burgdörfer, Phys. Rev. A **74**, 053417 (2006).
[5] F. L. Moore, J. C. Robinson, C. F. Bharucha, P. E. Williams, and M. G. Raizen, Phys. Rev. Lett. **73**, 2974 (1994); J. Ringot, P. Szriftgiser, J. C. Garreau, and D. Delande, Phys. Rev. Lett. **85**, 2741 (2000).
[6] L. Sirko, S. Bauch, Y. Hlushkshuck, P. M. Koch, R. Blümel, M. Barth, U. Kuhl, and H. J. Stöckmann, Phys. Lett. A **266**, 331 (2000).
[7] E. J. Galvez, B. E. Sauer, L. Moormann, P. M. Koch, and D. Richards, Phys. Rev. Lett. **61**, 2011 (1988).
[8] J. E. Bayfield, G. Casati, I. Guarneri, and D. W. Sokol, Phys. Rev. Lett. **63**, 364 (1989).
[9] M. Arndt, A. Buchleitner, R. N. Mantegna, and H. Walther, Phys. Rev. Lett. **67**, 2435 (1991).
[10] T. Gallagher and H. Maeda, Phys. Rev. Lett. **93**, 193002 (2004).
[11] S. Fishman, D. R. Grempel, and R. E. Prange, Phys. Rev. Lett. **49**, 509 (1982).
[12] A. Einstein, Ann. Phys. (Leipzig) **17**, 132 (1905).
[13] J. Gurian, H. Maeda, and T. Gallagher (private communication).
[14] M. W. Noël, M. Griffith, and T. Gallagher, Phys. Rev. A **62**, 063401 (2000).
[15] A. Krug and A. Buchleitner, Phys. Rev. A **66**, 053416 (2002).
[16] A. Buchleitner, D. Delande, and J. C. Gay, J. Opt. Soc. Am. B **12**, 505 (1995).
[17] J. H. Shirley, Phys. Rev. **138**, B979 (1965).
[18] Y. K. Ho, Phys. Rep. **99**, 1 (1983).
[19] A. Buchleitner, B. Grémaud, and D. Delande, J. Phys. B **27**, 2663 (1994).
[20] A. Krug and A. Buchleitner, Phys. Rev. A **72**, 061402(R) (2005).
[21] Our numerical threshold fields are extracted from the F dependence of the ionization yield as the fundamental experimental observable [15,16]. For all other parameters fixed, the relative numerical error $\Delta F_0^{10\%}$ is determined by the step size in F and is estimated on the order of few percent. This, as well as the weak dependence of $F_0^{10\%}$ on n_{eff} (which was fixed at $n_{\mathrm{eff}} = 270$ in our present calculations), leaves the significance of the structures observed in Figs. 1–3 qualitatively unaffected.For a related discussion, see A. Buchleitner and D. Delande, Chaos Solitons Fractals **5**, 1125 (1995).
[22] F. H. Faisal, *Theory of Multiphoton Processes* (Plenum, New York, 1987).
[23] We verified that our numerical thresholds in regime (III) deviate from semiclassical estimates of the one-photon threshold [24] by less than 30%. The discrepancy is due to the finite value of $n_{\mathrm{eff}} < \infty$.
[24] G. Casati, I. Guarneri, and D. L. Shepelyansky, IEEE J. Quantum Electron. **24**, 1420 (1988).
[25] A. Buchleitner, I. Guarneri, and J. Zakrzewski, Europhys. Lett. **44**, 162 (1998).
[26] R. Blümel and U. Smilansky, Z. Phys. D **6**, 83 (1987).
[27] R. Blümel, A. Buchleitner, R. Graham, L. Sirko, U. Smilansky, and H. Walther, Phys. Rev. A **44**, 4521 (1991).